PAPER • OPEN ACCESS

An optimized ensemble local mean decomposition method for fault detection of mechanical components

To cite this article: Chao Zhang *et al* 2017 *Meas. Sci. Technol.* **28** 035102

View the article online for updates and enhancements.

An optimized ensemble local mean decomposition method for fault detection of mechanical components

Chao Zhang[1,2]**, Zhixiong Li**[3,4,6]**, Chao Hu**[3,5]**, Shuai Chen**[1]**, Jianguo Wang**[1] **and Xiaogang Zhang**[2]

[1] School of Mechanical Engineering, University of Science and Technology of the Inner Mongol, Baotou 014010, People's Republic of China
[2] School of Mechanical and Manufacturing Engineering, University of New South Wales, Sydney, NSW 2052, Australia
[3] Department of Mechanical Engineering, Iowa State University, Ames, IA 50011, United States
[4] School of Mechatronic Engineering and Jiangsu Key Laboratory of Mine Mechanical and Electrical Equipment, China University of Mining and Technology, Xuzhou 221116, People's Republic of China
[5] Department of Electrical and Computer Engineering, Iowa State University, Ames, IA 50011, United States

E-mail: zhixiong@iastate.edu

CrossMark

Abstract

Mechanical transmission systems have been widely adopted in most of industrial applications, and issues related to the maintenance of these systems have attracted considerable attention in the past few decades. The recently developed ensemble local mean decomposition (ELMD) method shows satisfactory performance in fault detection of mechanical components for preventing catastrophic failures and reducing maintenance costs. However, the performance of ELMD often heavily depends on proper selection of its model parameters. To this end, this paper proposes an optimized ensemble local mean decomposition (OELMD) method to determinate an optimum set of ELMD parameters for vibration signal analysis. In OELMD, an error index termed the relative root-mean-square error (*Relative RMSE*) is used to evaluate the decomposition performance of ELMD with a certain amplitude of the added white noise. Once a maximum *Relative RMSE*, corresponding to an optimal noise amplitude, is determined, OELMD then identifies optimal noise bandwidth and ensemble number based on the *Relative RMSE* and signal-to-noise ratio (SNR), respectively. Thus, all three critical parameters of ELMD (i.e. noise amplitude and bandwidth, and ensemble number) are optimized by OELMD. The effectiveness of OELMD was evaluated using experimental vibration signals measured from three different mechanical components (i.e. the rolling bearing, gear and diesel engine) under faulty operation conditions.

(Some figures may appear in colour only in the online journal)

---

[6] Author to whom any correspondence should be addressed.

1. Introduction

Condition monitoring and fault diagnosis (CMFD) is an important research field in reliability analysis of mechanical components [1–3]. Many CMFD techniques have been developed to analyze the vibration signals acquired from these mechanical components [4–7]. Recently, time–frequency-domain analysis techniques, such as Wigner–Ville distribution [8] and wavelet transform [9–11], have attracted considerable attention. These techniques, shown to be successful in various applications, are, however, non-adaptive [12]. For example, wavelet analysis can extract local features in multiple scales, and hence enables the identification of singular components of a vibration signal for fault diagnosis of rotating machinery [8–11]. However, wavelet analysis has a critical limitation, i.e. different mother wavelets need to be determined or predefined for different signal processing applications. Therefore, these techniques are not self-adaptive [12].

Unlike the aforementioned analysis methods, empirical mode decomposition (EMD) can adaptively decompose any given complex signal into a series of intrinsic mode functions (IMFs) [13, 14]. However, one of the major disadvantages of EMD is its susceptibility to the mode mixing problem. Mode mixing is defined as either a single IMF consisting of multiple widely disparate scales, or a signal residing in multiple IMF components. Although ensemble empirical mode decomposition (EEMD) represents a significant improvement over EMD for reducing mode mixing [15–18], the performance of EEMD largely depends on proper determination of its model parameters (i.e. the ensemble number and the ratio of the added noise) [19]. In addition, the computation complexity is also a concern for EMD and EEMD [20, 21].

Recently, the local mean decomposition (LMD) [22] was introduced to solve the mode mixing problem in EMD. Instead of Hilbert transform, as is used in EMD, LMD uses smoothed local means to extract intrinsic modes from a signal. Hence, the information loss caused by Hilbert transform can be minimized [23]. The advantages of LMD over EMD were originally discussed in their applications to electroencephalogram (EEG) [22]. In mechanical fault detection, Wang *et al* [24, 25] used LMD for fault diagnosis of rotating machinery and demonstrated that LMD provided better performance than EMD. It was reported in [26] that the features extracted by LMD provided satisfactory fault detection performance on a helical gearbox. Kidar *et al* [27] compared LMD and EMD in gear fault diagnosis. Their analysis results suggested that LMD improved the detection effectiveness over EMD in early gear defects. Feng *et al* [28] adopted LMD to detect early faults in planetary gearboxes. Chen *et al* [29] applied LMD to detect both gear and bearing faults and showed LMD was more effective than EMD in fault detection. Liu *et al* [30] combined Wavelet transform and LMD to analyze field data obtained from a locomotive rolling bearing. Han and Pan [31] integrated LMD with entropy/energy ratio to detect rolling bearing faults. Wang *et al* [32] incorporated LMD into morphology analysis for pump fault diagnosis. The above mentioned studies demonstrate superior performance of LMD over EMD in mechanical fault diagnosis [24–32].

To further enhance the capability of LMD to mitigate mode mixing, Sun *et al* [33] recently presented the application of an ensemble LMD (ELMD) to gas leak detection. Similar to EEMD, ELMD adds white noise to a raw vibration signal when decomposing the signal into characteristic modes. Mode mixing caused by the uniform time–frequency distribution of different-scale components in the raw signal can be significantly reduced since the added white noise can assist in tuning the time–frequency distribution [34]. As a result, ELMD can often obtain more reliable smoothed local means than LMD [33, 34], and thus produce better performance in mechanical fault detection [34, 35]. Moreover, ELMD showed better performance than EEMD in terms of fault detection rate [33–35]. Because LMD is computationally more efficient than EMD [22], ELMD imposes less computational burden than EEMD.

The effectiveness of ELMD in mode-mixing reduction is often highly influenced by the selection of its parameters, i.e. the amplitude and bandwidth of the added noise and number of ensemble trials. Very limited work has been done to optimize these ELMD parameters, and no prior research has been found in mechanical fault diagnosis using parameter-optimized ELMD. Hence, it is worth investigating how the ELMD parameters affect the performance in fault diagnosis of mechanical components and how to optimize these parameters to achieve better performance. This paper proposes an optimized ensemble local mean decomposition (OELMD) method that optimizes three ELMD parameters (i.e. amplitude and bandwidth of the added noise, and number of the ensemble trials) to ensure satisfactory decomposition performance. Through the parameter optimization, the parameter dependency of the decomposition performance of ELMD can be accounted for when designing ELMD for a specific application. The resulting OELMD is expected to achieve a lesser degree of mode mixing than an ELMD with subjectively chosen parameters.

This work was inspired by the previous studies in [16, 18, 36]. In [18], Guo *et al* proposed a method based on the relative root-mean-square error (*Relative RMSE*) to optimize the noise level for EEMD. Lei *et al* [16] then presented the use of *Relative RMSE* to select both the sifting number and noise amplitude in EEMD. More recently, the *Relative RMSE*-based method was proposed in [36] for the optimization of the noise bandwidth in EEMD. To the best of the authors' knowledge, no prior studies have investigated the use of *Relative RMSE* as a criterion to optimize ELMD parameters. The contributions of this work include: (a) the development of a new procedure based on *Relative RMSE* to optimize the noise amplitude and bandwidth for ELMD; and (b) the adoption of signal-to-noise ratio (SNR) to select an appropriate ensemble number for ELMD. The effectiveness of OELMD were evaluated and compared with ELMD using experimental vibration data measured from three different mechanical components (i.e. the rolling bearing, gear and diesel engine).
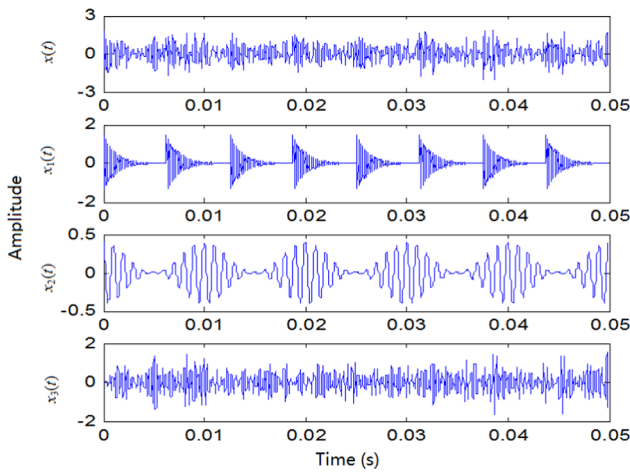
Figure 1. Time domain waveforms of the signal $x(t)$ and its components, $x_1(t)$, $x_2(t)$ and $x_3(t)$.

2. Fundamentals of the ELMD method

The ELMD method was recently developed to reduce mode mixing caused by the uniform time–frequency distribution of a signal. This method repeatedly applies LMD by adding white noise to the signal throughout the signal decomposition process [33]. If there are sufficient trials in the decomposition process, the added white noise can be canceled out in the final ensemble mean [34].

Assume that a multi-component nonlinear and/or non-stationary signal, $x(t)$, can be decomposed into a series of production functions (PFs), $PF_j(t)$, and a monotonic function $r_N(t)$ [22].

$$x(t) = \sum_{j=1}^{N} PF_j(t) + r_N(t) \tag{1}$$

where j is the index of the production function (PF), and N is the total number of the PFs. Essentially, each PF is the product of a purely frequency modulated signal and an envelope signal [22]. Furthermore, the corresponding complete time–frequency distribution can be obtained by assembling the instantaneous amplitudes and instantaneous frequencies of all PF components.

This process is demonstrated using a simulated signal $x(t)$ consisting of three components in equation (2).

$$x(t) = x_1(t) + x_2(t) + x_3(t) \tag{2}$$

where,

$$x_1(t) = 1.5 \times e^{-800t'} \times \sin(2\pi \times 5000t) \tag{3}$$

$$x_2(t) = 0.2 \times (1 + \cos(2\pi \times 100t)) \times \cos(2\pi \times 1000t) \tag{4}$$

and $x_3(t)$ is an additive Gaussian white noise with the bandwidth from 2 to 4 kHz. In equation (3), t' is a periodic function of time with a fundamental period of 1/160 s. This frequency range was selected based on the fact that, compared to low-frequency noises, high-frequency noises generally have more contributions to the changes of the extremum distribution of the original signal [24]. The time domain waveforms of $x(t)$ and its three components are shown in figure 1, where the sampling frequency is 40 kHz.
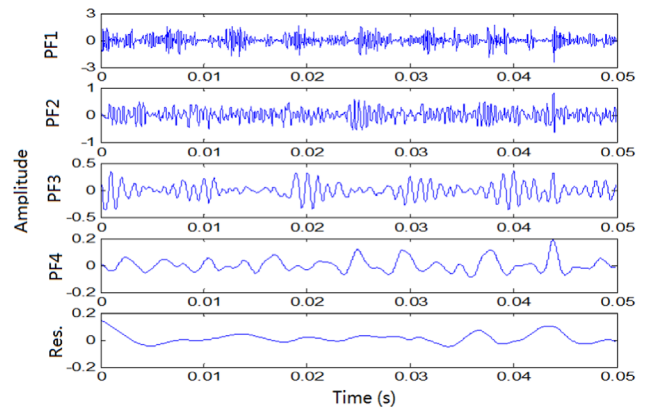

Figure 2. ELMD analysis results on the simulated signal shown in figure 1. The bottom figure shows the residual from the decomposition.

The decomposition results of $x(t)$ by ELMD are shown in figure 2, where it can be observed that the four PFs (i.e. PF1–PF4) with different characteristic modes do not well match the actual modes shown in figure 1. The reason is probably that improper ELMD parameters were used in this analysis (the amplitude and bandwidth of the added noise and the ensemble number were subjectively chosen, as is typically done in the original ELMD method). Hence, properly determining the ELMD parameters is expected to improve the decomposition performance.

In the ELMD decomposition process, if the amplitude of the added noise is much larger than that of the original signal, it may result in redundant PFs that consume extra computational time. In contrast, if the amplitude of the added noise is too small, the noise may not affect the extremums that the LMD method relies on [35]. Thus, the effectiveness in mode mixing reduction may dramatically decrease. In addition, high-frequency noises have more impact on the changes of the extremum distribution of the original signal than low-frequency noises [34]. However, the computation complexity increases with the increase of the noise bandwidth. Finally, if the number of ensemble trials is too large, the computational cost may be prohibitively high. Conversely, a very small value may not be sufficient to cancel out the noise remaining in each PF [33]. Therefore, it is important to be able to determine optimum ELMD parameters that ensure effective mitigation of mode mixing and minimize the computational cost. It is worth noting that most of the existing studies on ELMD designed ELMD with subjectively selected parameters that are often suboptimal. Hence, there is a need for a systematic and effective approach to selecting suitable ELMD parameters.

3. Optimized ensemble local mean decomposition (OELMD)

Optimization of the added white noise's amplitude (L_N) and bandwidth (f_b) and the ensemble number (N_E) is essential to reduce mode mixing and can lead to a reduced computational cost as well. Here, OELMD is proposed to accomplish parameter optimization.
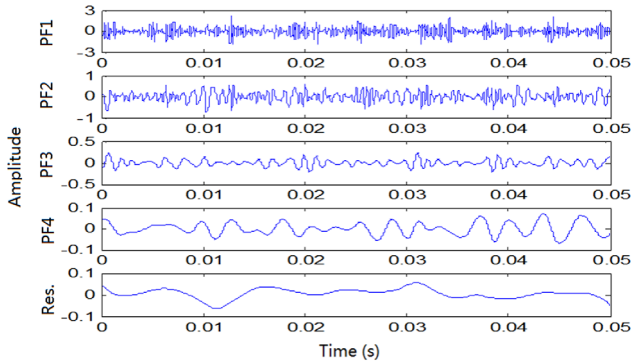
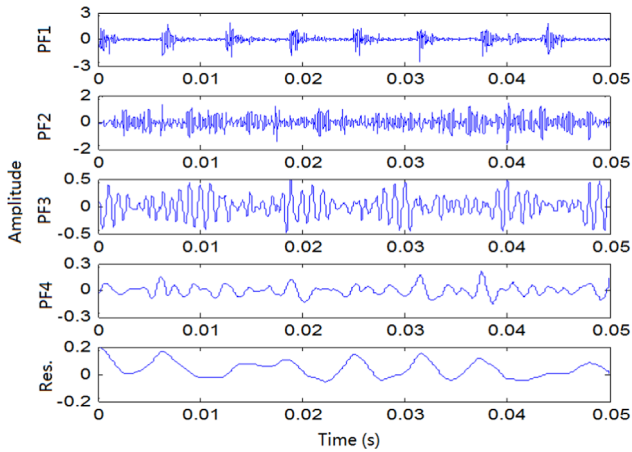**Figure 3.** Decomposition result with a noise amplitude of 0.1.

Figure 4. Decomposition result with a noise amplitude of 0.6.

3.1. Optimization of noise amplitude

Initially, the effects of the added noise's amplitude on ELMD were investigated. For $x(t)$ described in equation (2), figures 3–5 illustrate the decomposition results using ELMD with noise amplitudes of 0.1, 0.6, and 1.5, respectively. The number of ensemble trails was subjectively set to 100 in these simulations.

    As can be seen in figures 3–5, the degree of mode mixing varies with the amplitude of the added noise. When the amplitude of the added noise is 0.1 (figure 3), the components $x_1(t)$ and $x_2(t)$, cannot be separated by the first two PFs because of mode mixing. When the amplitude is 1.5, the mode mixing effect in figure 4 is worse than that in figure 3. In comparison, when the amplitude of the added noise is 0.6, the mode mixing effect in figure 5 is less than those in figures 3 and 4. The PFs in figure 5 correspond to the original $x(t)$ components (i.e. PF$_1$, PF$_2$ and PF$_3$ correspond to $x_1(t)$, $x_2(t)$ and $x_3(t)$, respectively). These observations are consistent with [33], where the noise amplitude was suggested to be neither too small nor too large.

    In order to choose a suitable noise amplitude value, inspired by [16–18], an error index, termed relative root-mean-square error (*Relative RMSE*), is introduced in this work. *Relative RMSE* is defined as the ratio of the root-mean-square of the decomposition error to the root-mean-square of the original signal $x(t)$, where the decomposition error is the difference between $x(t)$ and a specific PF, $c_{max}(t)$,
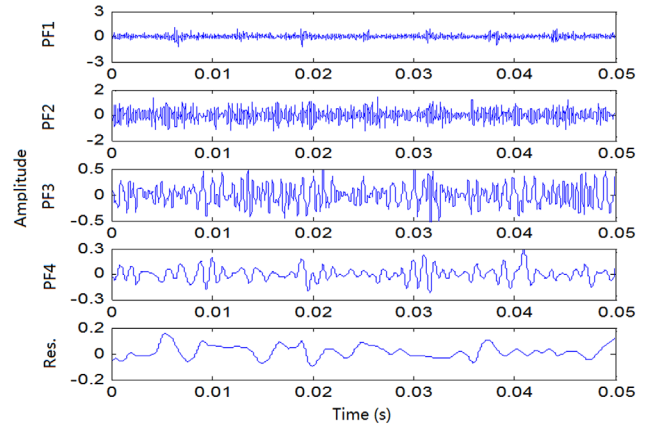

Figure 5. Decomposition result with a noise amplitude of 1.5.

i.e. the PF component with the highest correlation with the original signal [17]. Mathematically, the *Relative RMSE* can be expressed as [17, 18]:

$$Relative\ RMSE = \sqrt{\frac{\sum_{k=1}^{M}(x(k) - c_{max}(k))^2}{\sum_{k=1}^{M}(x(k) - \bar{x})^2}} \quad (5)$$

where $x(k)$ is the kth sample in $x(t)$, M is the total number of samples in $x(t)$, and $\bar{x}$ is the sample mean of $x(t)$. On the one hand, if the *Relative RMSE* is close to zero, it indicates that the specific PF, $c_{max}(t)$, is similar to the original signal. This suggests that $c_{max}(t)$ contains not only the main component in the original signal but also noise and/or other weakly correlated or irrelevant signal components [12]. In other words, mode mixing occurs in this PF. On the other hand, an optimum value of noise amplitude that maximizes the *Relative RMSE* may exist. At this optimum value, the PF is close to an intrinsic mode/component of $x(t)$. To this end, an optimization method was proposed to determine the appropriate noise amplitude by maximizing the *Relative RMSE*.

    The relationship between the *Relative RMSE* and the added noise amplitude L_N for $x(t)$ is given in figure 6, where L_N was initially set to a maximum value $l_{max} = 2$, and then decreased to a minimum value l_{min} in increments (Δl) of 0.05. As can be seen in the figure, the maximum *Relative RMSE* corresponds to 0.6 of the noise amplitude. In figures 3–5, the decomposition performance of ELMD at the noise amplitude of 0.6 is better than at 0.1 or 1.5. Hence, the proposed optimization approach based on the maximum *Relative RMSE* is effective to find a suitable noise amplitude value. Figure 6 also indicates that the maximum *Relative RMSE* under different ensemble numbers N_E is different, but the optimal noise amplitude remains the same. Therefore, the ensemble number hardly affects the determination of the noise amplitude.

3.2. Optimization of noise bandwidth

The noise bandwidth is another factor that influences the decomposition performance of ELMD. As with the selection of noise amplitude, the noise bandwidth is optimized by
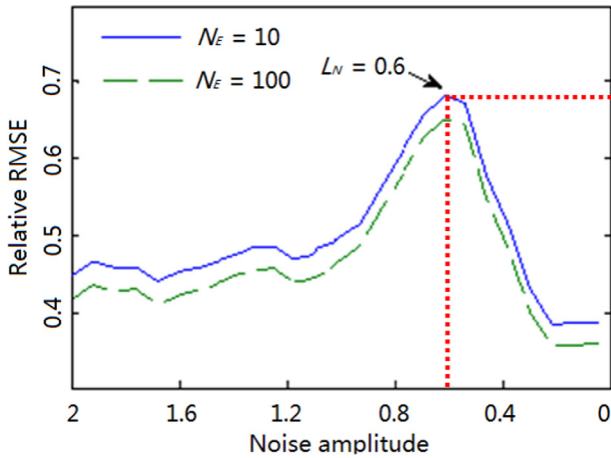
Figure 6. Relationship between *Relative RMSE* and the noise level of the added white noise.

Figure 7. Relationship between *Relative RMSE* and the upper bandwidth of added noise.

maximizing the *Relative RMSE* [17]. The detailed procedure is as follows:

First, define a pool of candidate upper bandwidths of the added noise, $f_b = i \times f_s$, $i = 1, 2,..., n$, where f_s is the sampling frequency of $x(t)$ in equation (2).

Second, obtain the interpolated signal $x'(t)$ of $x(t)$ by cubic spline interpolation for each candidate f_b. The data length of $x'(t)$ is equal to the length of $x(t)$ with the same f_b.

Third, perform ELMD on $x'(t)$ for each candidate f_b with the optimal noise amplitude determined in section 3.1. The upper bandwidth of the added white noise is f_b in the ELMD process. Then, calculate the *Relative RMSE* values for each candidate f_b.

Finally, determine the optimal f_b as the candidate with the maximum *Relative RMSE*.

Figure 7 shows the simulation results of ELMD on $x(t)$ using different f_b values. As can be seen in this figure, the maximum *Relative RMSE* is located at 40 kHz, which is selected as the optimal noise bandwidth. As was the case in figure 6, the location of the maximum *Relative RMSE* is not influenced by N_E.

In order to verify the optimization result in figure 7, figure 8 illustrates the decomposition performance of ELMD on $x(t)$ with different noise bandwidths. Figure 8(a) shows that the PFs well match the original $x(t)$ components because the optimal noise bandwidth of 40 kHz is used. In figure 8(b), significant mode mixing is observed when the noise bandwidth is 80 kHz because the *Relative RMSE* at 80 kHz in figure 7 is the local minimum. In figure 8(c), when the noise bandwidth is 120 kHz, a redundant mode PF3 appears, indicating mode mixing. Similar results are observed in figure 8(d) when the upper bandwidth of the added noise is 200 kHz. Figures 8(c) and (d) indicate that the decomposition using 120 kHz provides better performance than that using 200 kHz. This is because the *Relative RMSE* at 120 kHz is larger than that at 200 kHz. Since a 40 kHz bandwidth produces the largest *Relative RMSE* in figure 7, the decomposition results in figure 8(a) are superior to those of the other three bandwidths. Consequently, figure 8 demonstrates the effectiveness of the optimization method.
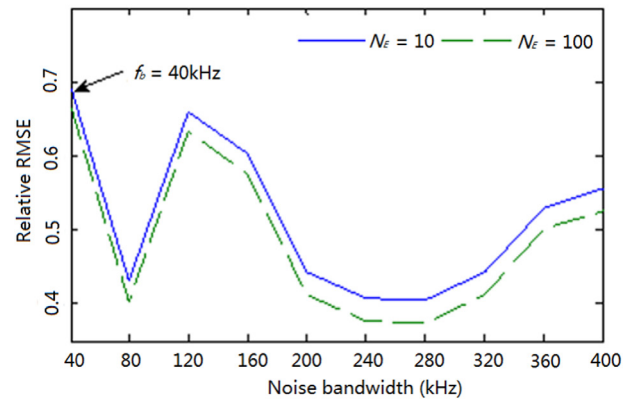
3.3. Optimization of number of ensemble trials

The number of ensemble trials needed is proportional to the amount of white noise added to the original signal [15]. After determining the optimal noise amplitude and bandwidth, the next task is to choose an appropriate number of ensemble trails. If the number is too large, it may lead to a prohibitively high computational cost [33]. Conversely, a small value may not be enough to cancel out the added noise from the decomposed PFs. In this work, the signal-to-noise ratio (SNR) was adopted to determine the appropriate ensemble number.

For each ensemble number in ELMD, the signal decomposition stops once the selected PF is obtained. Here, the first PF was used to calculate the SNR value and find the appropriate ensemble number.

$$\text{SNR} = 10\log_{10}(p_1/p_2) \tag{6}$$

Here, p_1 is the power of the first PF, and p_2 is the power of the noise, which is equal to the power of the original signal minus p_1. The relationship between the SNR and the ensemble number, as shown in figure 9, was obtained by analyzing $x(t)$ using ELMD with the optimized noise amplitude of 0.6 and bandwidth of 40 kHz.

As can be seen in figure 9, when the ensemble number is smaller than 100, an increase in the ensemble number leads to a significant increase in the SNR value. However, after 100 ensemble trials, the SNR value remains constant. Therefore, the optimal ensemble number for $x(t)$ when the optimized noise amplitude of 0.6 and bandwidth of 40 kHz are used is 100.

Figure 10 compares the decomposition performances of ELMD for both 20 and 100 ensemble trials. The original $x(t)$ components of the decomposed PFs are recovered correctly in both cases. In order to compare the results of different ensemble trials quantitatively, two evaluation indexes, namely the correlation coefficient r and the energy error E, are introduced. Coefficient r refers to the correlation between the original $x(t)$ components and the PFs decomposed by ELMD. The energy error, E, is defined as:

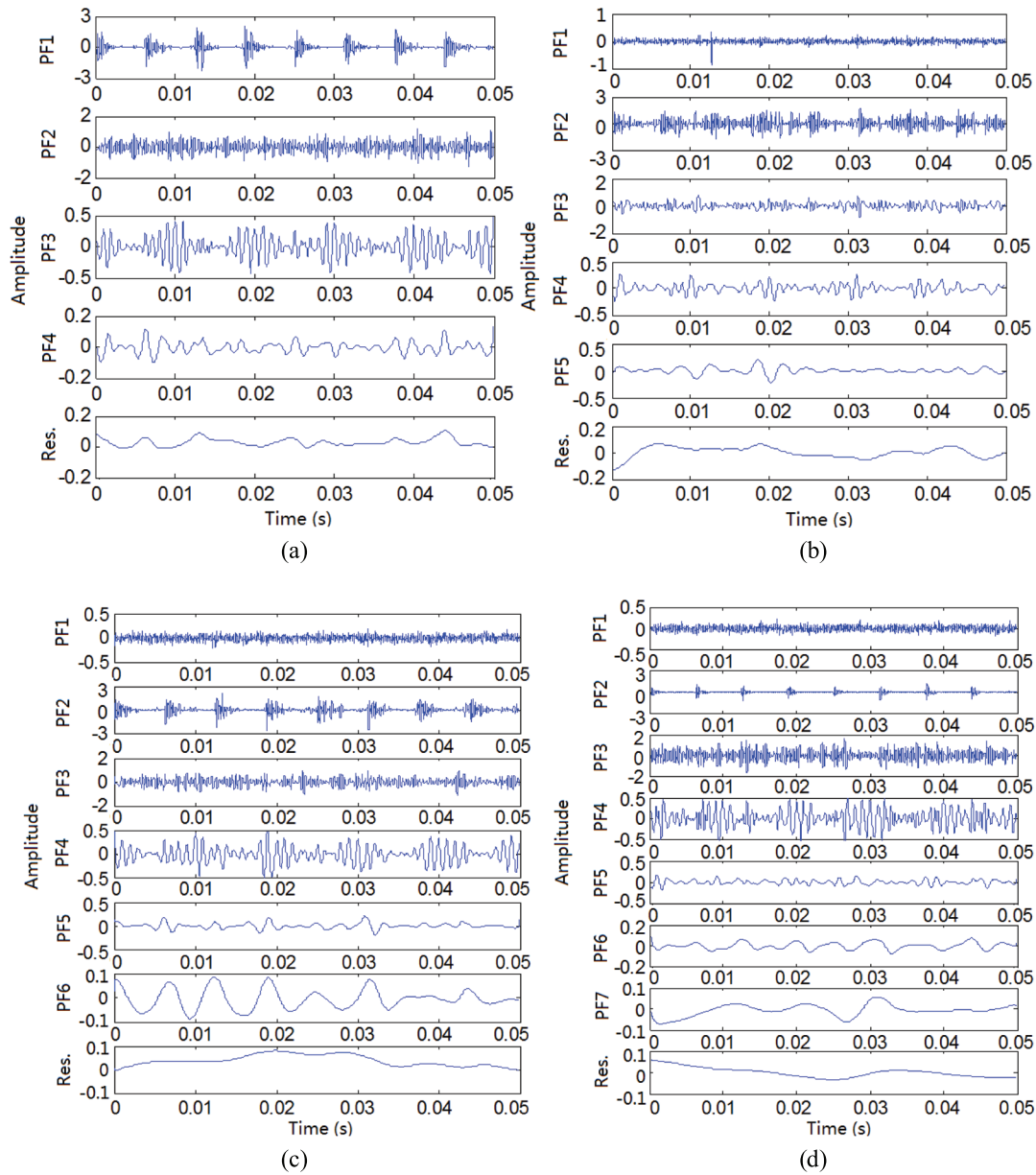$$E_i = \frac{E_s(x_i(t) - I_i)}{E_s(x_i(t))} \tag{7}$$

Figure 8. Decomposition results of ELMD on $x(t)$ with different noise bandwidths. (a) $f_p = 40\,\text{kHz}$ (b) $f_p = 80\,\text{kHz}$. (c) $f_p = 120\,\text{kHz}$ (d) $f_p = 200\,\text{kHz}$.
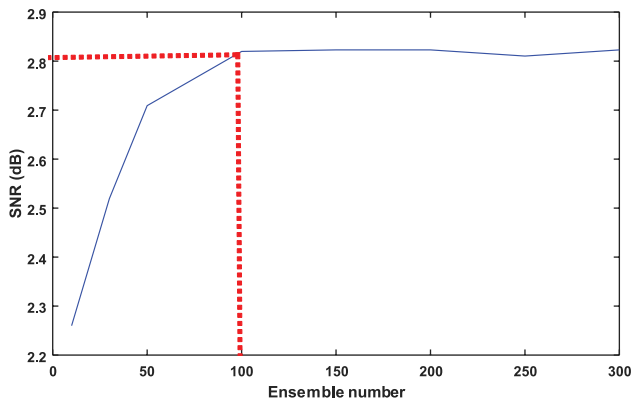

Figure 9. Relationship between SNR and the number of ensemble trials.

where $E_s(\cdot)$ is the energy of the signal, $x_i(t)$ is the ith original component of $x(t)$, and I_i is the corresponding PF of $x_i(t)$. In this simulation, $i = \{1, 2, 3\}$. A smaller E indicates a better decomposition performance of ELMD. Table 1 lists r and E for different numbers of ensemble trials with the optimized noise amplitude of 0.6 and bandwidth of 40 kHz. The quantitative indexes r and E are shown for $x_1(t)$ and $x_2(t)$. As the number of ensemble trials increases, r increases, indicating improved ELMD performance. The correlation coefficient of ELMD for 100 ensemble trials is larger than for 20 trials, suggesting better decomposition performance in that case. However, as the number of ensemble trials increases over 100, the gain in ELMD performance is very limited (i.e. less than 0.0012). Similar results are also observable for E. Because the computation effort needed for 200 ensemble trials is twice
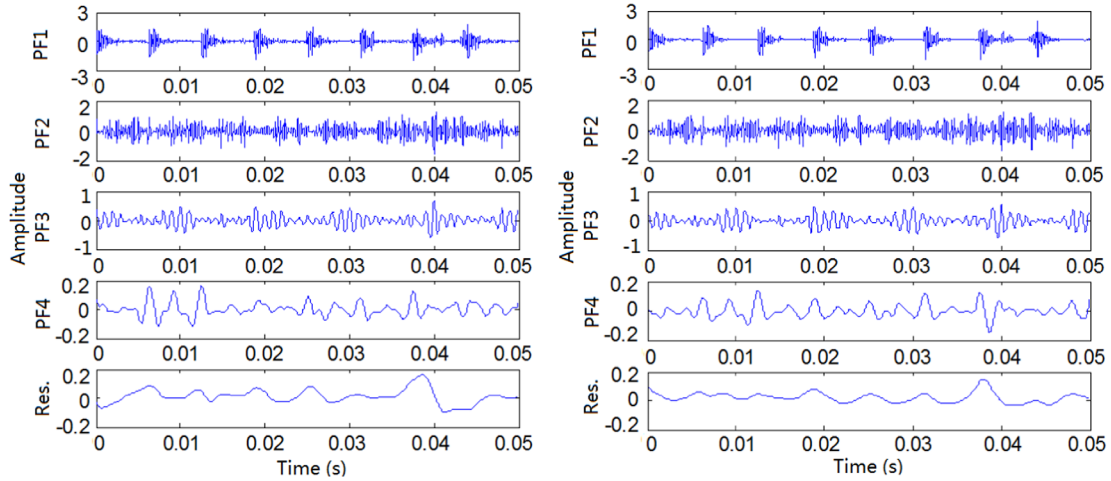
Figure 10. Results of decomposition by ELMD for $N_E = 20$ (left) and $N_E = 100$ (right).

Table 1. Decomposition performance for different numbers of ensemble trials.

N_E	r_1	r_2	E_1	E_2
20	0.8212	0.8199	0.4143	0.3627
50	0.8415	0.8237	0.4124	0.3611
100	0.8495	0.8398	0.3981	0.3568
150	0.8502	0.8403	0.3977	0.3566
200	0.8507	0.8405	0.3972	0.3563

that needed for 100 trials, it is reasonable to choose 100 as the optimal number of trials for this specific case. Therefore, the optimized ensemble number in figure 9 is verified, and SNR is shown to be an effective criterion for determining the ensemble number.

3.4. Procedure of OELMD

Figure 11 shows a flowchart of the proposed OELMD method. For a given signal $x(t)$, the decomposition process for the proposed OELMD method can be summarized as follows:

Step 1—Determine the optimal noise amplitude and bandwidth using maximum *Relative-RMSE* based optimization (see sections 3.1 and 3.2).

Step 2—Calculate the appropriate number of ensemble trials with the SNR-optimization approach using the optimal noise amplitude and bandwidth (see section 3.3).

Step 3—Perform ELMD with the optimized parameters (i.e. optimal noise amplitude, bandwidth, and ensemble number).

It is worth noting that Step 1 determines the optimal noise amplitude and bandwidth sequentially and separately, and an alternative to the sequential optimization is to jointly optimize both parameters by solving the following optimization problem: $L_N^*, \quad f_b^* = \arg\max_{L_N, f_b} \text{Re}lative\ RMSE(L_N, f_b; x(t), N_E)$. One way to solve this problem is to use an iterative two-step optimization algorithm that iterates between the optimization of L_N (keeping f_b fixed) and the optimization of f_b (keeping L_N fixed) until a convergence criterion is met. A detailed discussion of

the joint optimization is beyond the scope of this work, and will be considered in our future work.

After the three parameters of the white noise were optimized, a comparison of the ELMD ($L_N = 0.2$, $f_b = 80\,\text{kHz}$ and $N_E = 200$) and OELMD ($L_N = 0.6$, $f_b = 40\,\text{kHz}$ and $N_E = 100$) methods was conducted. The decomposition results of the same original signal $x(t)$ derived by ELMD and OELMD are presented in figure 12. It can be seen that OELMD performs well in the elimination of mode mixing. For further comparison, the envelope spectra of the decomposed components are respectively presented in figure 13. In figure 13, the envelope spectra of the first two components, obtained by ELMD and OELMD, are similar. In the OELMD results, the spectrum lines of the high frequency (156 Hz) and low frequency (98 Hz) components appear distinct. However, the amplitudes of these two components (98 Hz and 156 Hz) in the ELMD results are smaller than in the OELMD results, and the frequency multiplication components in the ELMD results are less distinguishable than in the OELMD results. Overall, the spectrum lines in the OELMD results are more clearly visible than in the ELMD results, where a serious frequency interference problem exists. Consequently, OELMD was superior to ELMD in term of reducing mode mixing in this simulation.

4. Experimental results and discussion

To verify the effectiveness of the proposed OELMD method in mechanical fault diagnosis, experimental data collected from three different mechanical components was analyzed. The performances of OELMD and ELMD were compared in the experimental analysis.

4.1. Case study 1: bearing fault detection

The first test case was detection of an inner race fault of a rolling bearing. The bearing vibration signal was collected from a gearbox test rig (figure 14), which consisted of one planetary and one parallel gearbox, a 3 hp driving motor, and a magnetic brake. A local pitting defect was introduced into
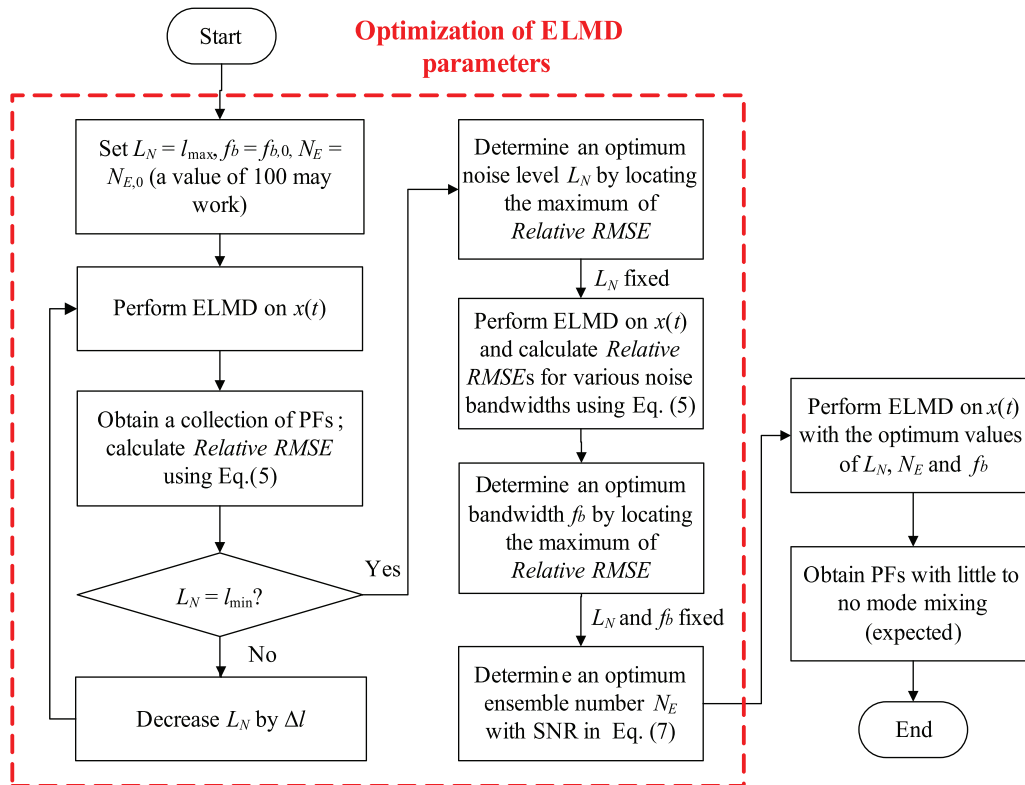
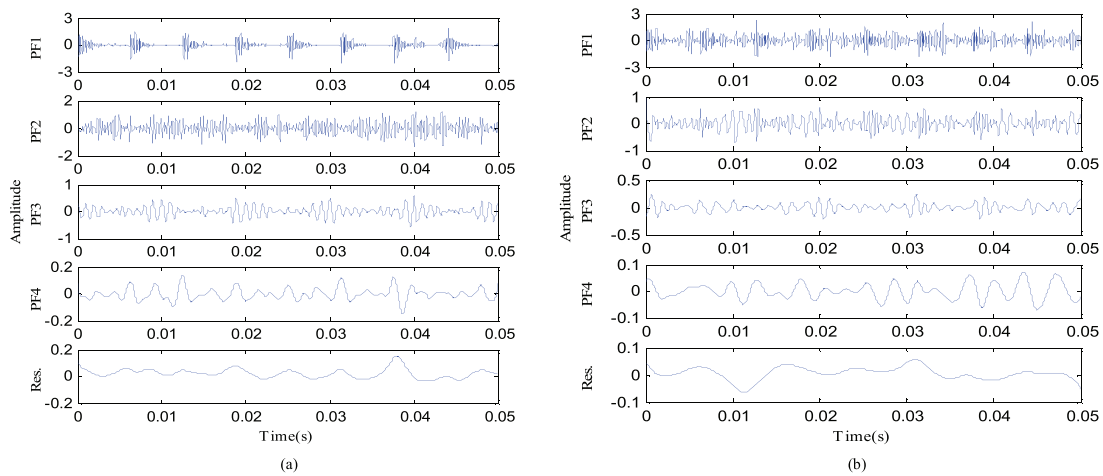**Figure 11.** Flowchart of the OELMD method.

Figure 12. Decomposition results of the simulated signal $x(t)$ by the OELMD and ELMD methods. (a) Decomposition results of OELMD (b) Decomposition results of ELMD.

the inner race of the bearing in the input shaft of the planetary gearbox (figure 14). A number 9 ball bearing with a diameter of 7.925 mm, pitch diameter of 38.989 mm, and contact angle of 0° was used. An accelerometer recorded the bearing vibration. The motor driving speed was 1750 rpm and the sampling frequency was 12 000 Hz. Thus, the rotating frequency of the input shaft of the parallel gearbox was $f_r = 29.17$ Hz, and the ball pass frequency of the inner race (BPI) was $f_i = 157.93$ Hz.

Figure 15 illustrates the raw vibration signal of the faulty bearing. Obvious bearing impulsive and gear modulation components were observed in the raw vibration (figure 15). The OELMD was then applied to the raw vibration signal.

The parameter optimization results are shown in figure 16. As can be seen in the figure, the optimal noise amplitude in figure 16(a) is 0.3, the optimal noise bandwidth in figure 16(b) is 12 kHz, and optimal ensemble number in figure 16(c) is 100.

Figures 17 and 18 depict the time and envelope waveforms of the PFs decomposed by OELMD. Four dominant frequency components located at the harmonics of BPI (i.e. f_i, $2f_i$, $4f_i$, and $5f_i$) can be observed in the first PF in figure 18. A pure dominant frequency at BPI is observed in PF3, but in PF4, the only dominant frequency is at $3f_r$. As a result, the vibration modes of the input shaft rotation and the inner race were decomposed into different PFs according to figure 18. Although in PF2 in figure 18, the two modes ($2f_r$ and $4f_i$) mix,
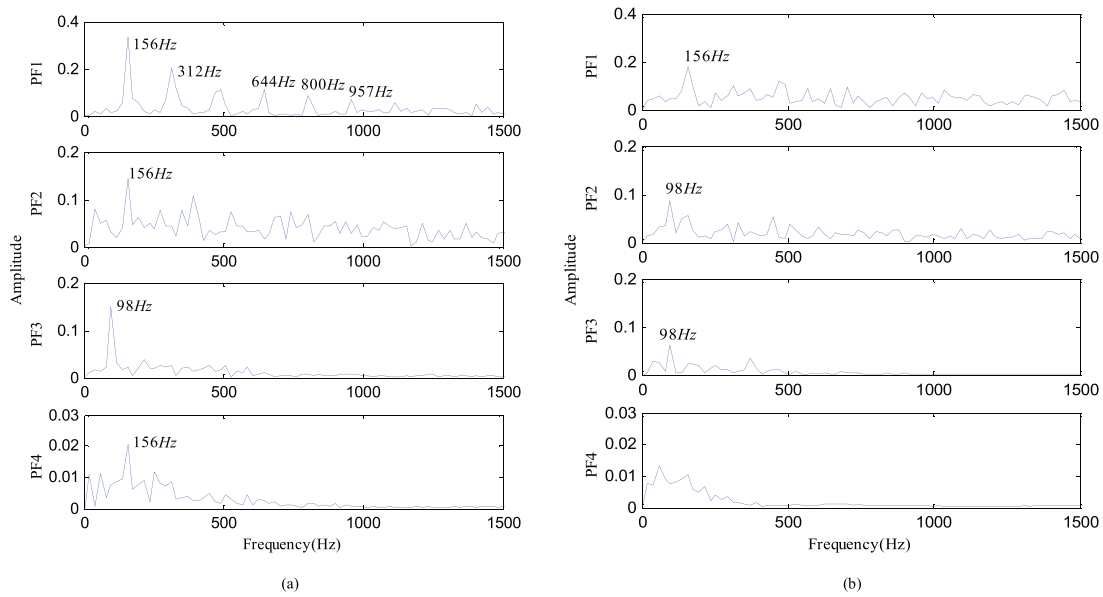
(a)   (b)

Figure 13. The envelope spectrum of the PFs derived by the OELMD and ELMD methods from the simulated signal $x(t)$. (a) The envelope spectrum of PFs by OELMD. (b) The envelope spectrum of PFs by ELMD.
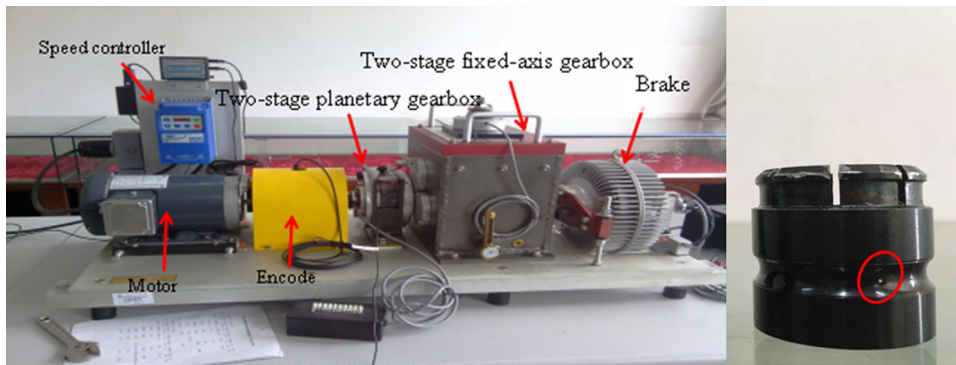

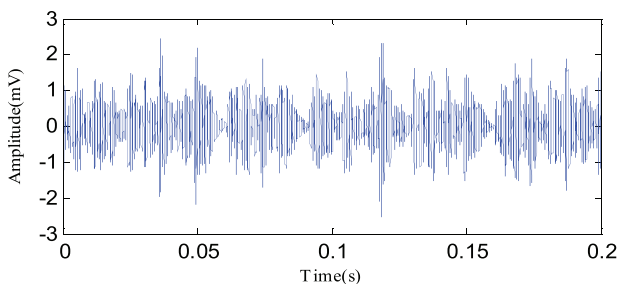**Figure 14.** Experimental setup and the faulty bearing with inner race defect.

Figure 15. Raw vibration signal of the tested bearing with inner race fault.

when comparing the amplitude of PF1 and PF2, it is obvious that the peak values of the dominant frequency components in PF1 are much larger than that of those in PF2. PF1 is the most informative mode of the three. According to Randall [37], for a bearing with an inner race defect, the main vibration pattern in the envelope spectrum of the bearing vibration will be a series of peaks at BPI harmonics. Therefore, OELMD analysis correctly identified the inner race fault (figure 18).

A comparative study was performed on the OELMD and ELMD methods. The time and envelope waveforms of the PFs decomposed by ELMD are presented in figures 19 and 20.

The ELMD parameters were selected as follows: the noise amplitude was 0.1, the noise bandwidth was 20 kHz, and the ensemble number was 100. ELMD (figure 20) suffered much more severe mode mixing than OELMD (figure 18) did. For EMLD, the two modes ($2f_r$ and $4f_i$) mixed in PF1 and PF3. In addition, PF2 and PF4 were useless modes since they did not provide any useful information on the bearing vibration. In addition, the largest peak value of PF1 in figure 20 was located at $2f_r$, while in figure 18, the first PF obtained by OELMD contained only BPI harmonics. Overall, this comparison suggests that (a) because of unsuitable parameters, the ELMD method is subject to severe frequency interference, and (b) the fault detection performance of OELMD is better than that of ELMD.

4.2. Case study 2: gear fault detection

The second test case was detection of gear wear faults in the parallel gearbox (figure 14). Figure 21 shows the structure diagram of the gearbox. The wear fault was introduced to the driving gear $Z2$. The motor driving speed was 980 rpm, and the sampling frequency was 12 000 Hz. The transmission ratio of the planetary gearbox was 12.64, and the fault characteristic
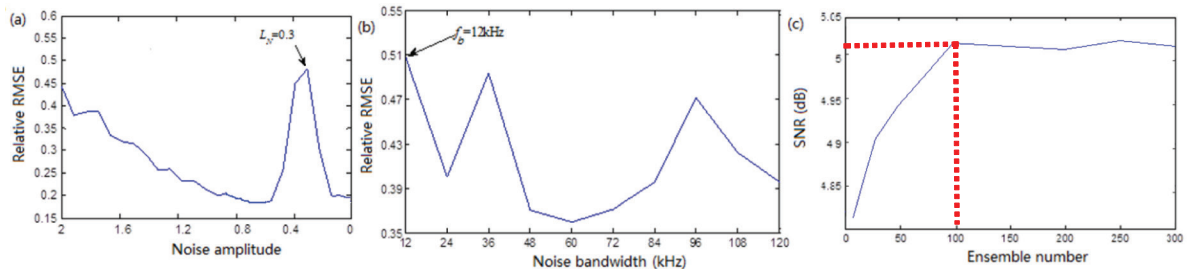
Figure 16. OELMD parameter optimization results: (a) noise amplitude, (b) noise bandwidth, and (c) ensemble number.
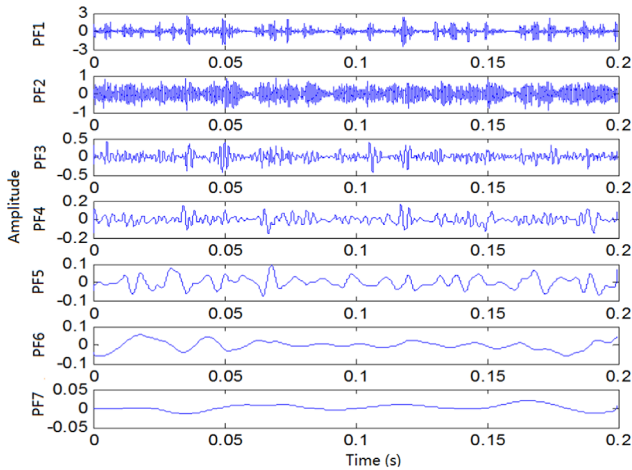

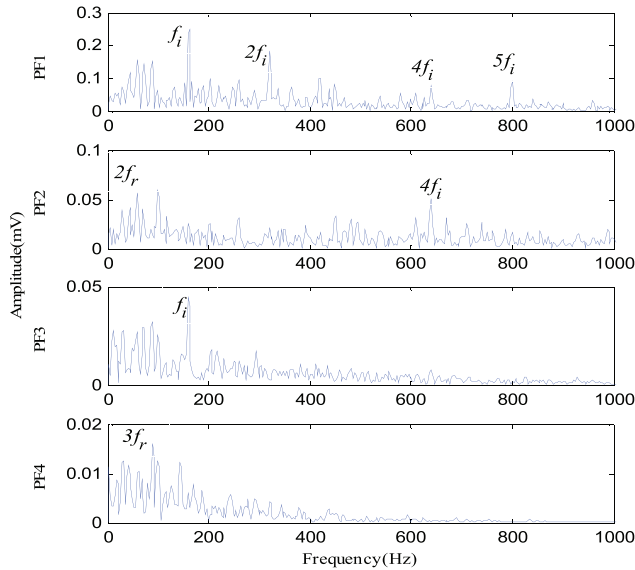**Figure 17.** Time waveforms of the PFs decomposed by OELMD.

Figure 19. Time waveforms of the PFs decomposed by ELMD.

Figure 18. Envelope waveforms of the PFs decomposed by OELMD.

Figure 20. Envelope waveforms of the PFs decomposed by ELMD.
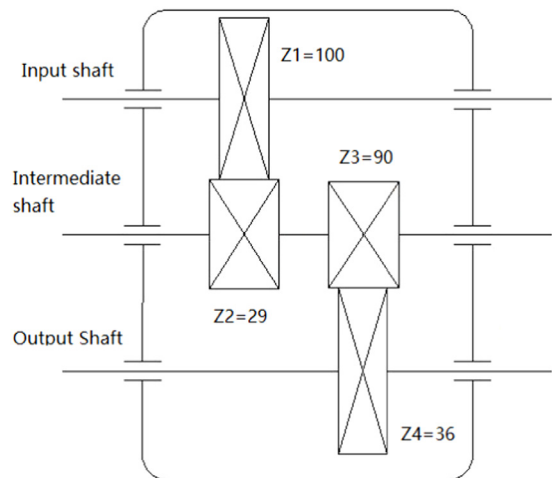
Figure 21. The structure diagram of the parallel gearbox in figure 12.

frequency and meshing frequency of $Z2$ were $f_r = 4.46$ Hz and $f_z = 129.21$ Hz respectively.

Figure 22 shows the time and frequency spectra of the raw gear vibration signal. In figure 22(b), frequency peaks appear at 129.67, 389.01, and 907.69 Hz (i.e. f_z, $3f_z$ and $7f_z$), indicating that the meshing frequency of the $Z1$–$Z2$ gear pair dominates the vibration response of the parallel gearbox. OELMD was then applied to the raw vibration signal. Figure 23 shows the parameter optimization results. As indicated in the figure,
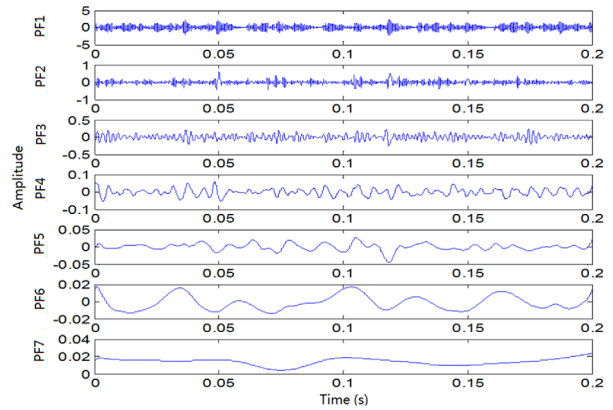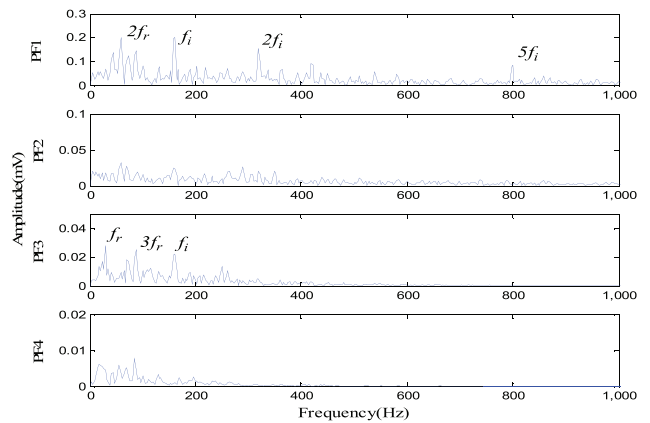
Figure 22. The raw vibration signal: (a) the time domain waveform and (b) the frequency spectrum.

Figure 23. OELMD parameter optimization results: (a) noise amplitude, (b) noise bandwidth, and (c) ensemble number.

Figure 24. Time waveforms of the PFs decomposed by (a) OELMD and (b) ELMD.

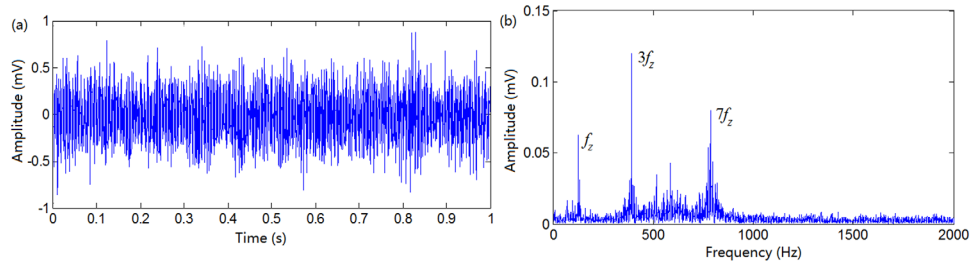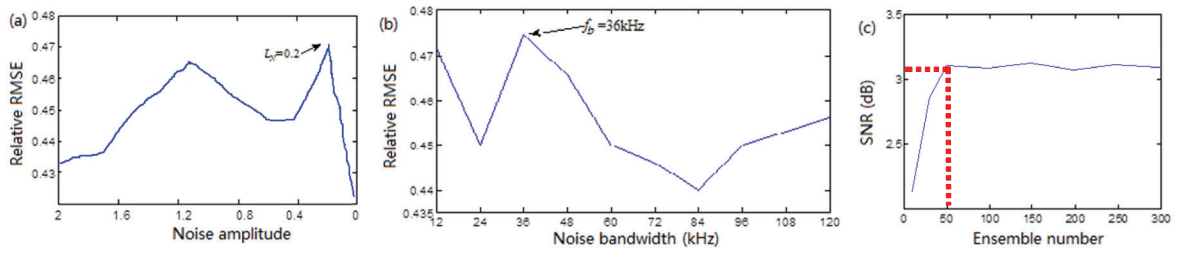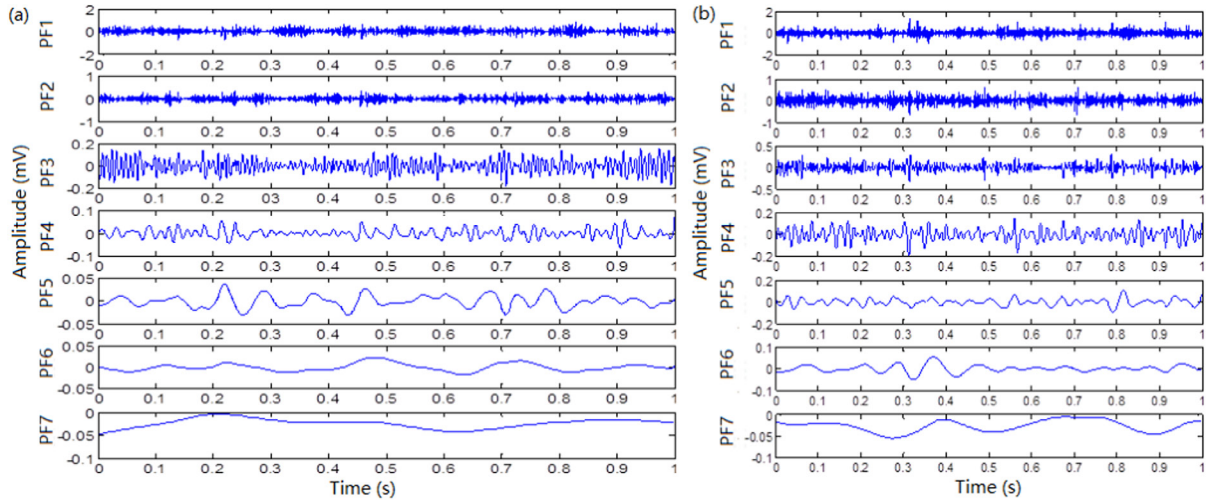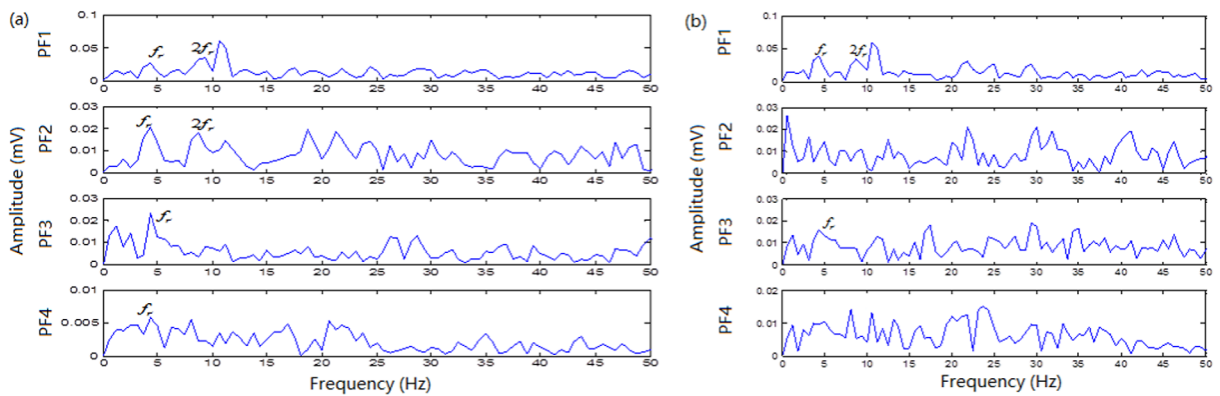**Figure 25.** Envelope waveforms of the PFs decomposed by (a) OELMD and (b) ELMD.

Figure 26. The installation positions of the accelerometers.

the optimal noise amplitude in figure 23(a) is 0.2, the optimal noise bandwidth in figure 23(b) is 36 kHz, and optimal ensemble number in figure 23(c) is 50.

Figures 24 and 25 show the results of analysis on OELMD and ELMD side by side. For ELMD, the noise amplitude was 0.1, the noise bandwidth was 30 kHz, and ensemble number was 50. As indicated in figure 24, there are no significant differences between OELMD and ELMD in the time waveforms. However, in figure 25(a) distinct frequency components of f_r and $2f_r$ are visible in PF1 and PF2 (decomposed by OELMD), whereas in figure 25(b), PF1 alone demonstrates these frequency components (using ELMD). In addition, in figure 25(b), PF2 and PF4 fails to provide any information about the fault frequency f_r of gear *Z*2. The results indicate better performance of OELMD than ELMD in the gear fault detection.

4.3. Case study 3: valve fault detection of a diesel engine

A four-stroke, four-cylinder diesel engine (Model 4135D) was tested to evaluate the proposed OELMD method. The engine operating rotating speed was 1500 rpm, and its operating power was 50 kW. In the experiment, the inlet valve clearance of the first cylinder was set to a large value to simulate a valve fault condition. Four piezoelectric accelerometers were installed on the right-side engine bodies of the four cylinders to measure their vibration signals (figure 26). A sampling frequency of 30 kHz was used. Cylinder vibration was measured under normal and valve fault conditions.

The measured raw vibration of the first cylinder was used for the analysis. Figure 27 shows the time and frequency spectra of the raw diesel vibration signals under normal and valve fault conditions. The time waveforms in figures 27(a) and (b) are similar with the exception of an approximately 0.01 s lag time between the normal and faulty waveforms. On the other hand, diesel engine vibration was much more intense under the valve fault condition than under normal conditions. The largest peak value under valve fault condition reached 200 mV while the largest peak under normal condition reached less than 150 mV. Additionally, there was a period of severe vibration impulses from 0.056 s to 0.060 s (figure 27(a)). In the corresponding period of the normal waveform in figure 27(b), there was no such severe vibration. It is reasonable to conclude that the valve fault may have generated these vibration impulses.

In the frequency spectra in figures 27(c) and (d), the dominant frequency peaks for both normal and valve fault conditions appear at 3545 Hz. This 3545 Hz vibration pattern is probably the first order harmonic of the diesel engine's natural vibration mode. The dominant peak is much higher under the valve fault condition than under normal conditions, which is consistent with the time waveforms in figures 27(a) and (b). The frequency spectra also demonstrate that under the valve fault condition, the diesel engine's main vibration components come from the frequency range of 3000 Hz–4000 Hz. The vibration contributions under normal conditions exist in a broader frequency range (2000 Hz–4000 Hz) than those under the valve fault condition.

OELMD was then applied to decompose the raw vibration signal into seven PFs. In the analysis, optimal values for noise amplitude (0.36), noise bandwidth (59 kHz), and ensemble number (150) were used. Figures 28 and 29 show the OELMD analysis results. For ELMD, noise amplitude of 0.2, bandwidth of 50 kHz, and ensemble number of 150 were used.

OELMD and ELMD provide almost the same decomposition result on the first PF (figure 28). In the range of 3000 Hz–4000 Hz, the frequency spectra of PF1 for both OELMD and ELMD (figure 29(a) and (b)) and the raw fault vibration signal (figure 27(c)) are similar. Since the dominant peaks of the two PF1 modes in figures 29(a) and (b) are located at 3545 Hz, according to the results of the analysis in figure 27, it is reasonable to conclude that PF1 best represents the overall tendency of the diesel engine vibration.

However, in figure 28, the second PF decomposed by OELMD differs from the one decomposed by ELMD. OELMD provides clear impulsive components in PF2, while ELMD does not show many individual impulses. The frequency spectra of these second PFs reveal that the PF2 decomposed by OELMD has an absolute dominant frequency at 3640 Hz (figure 28). In contrast, the ELMD-decomposed PF2 has two dominant frequency components: one at 3640 Hz and the other in a mixing mode. The third PF obtained by OELMD also contains one dominant frequency at 3640 Hz (figure 29(a)), although a disturbance frequency component is present as well. However, the dominant frequency component of PF3 obtained by ELMD is located at 1384 Hz (figure 29(b)), which does not belong to the primary vibration frequency range (3000 Hz–4000 Hz) for the diesel engine with a valve fault. As a result, the PF3 obtained by OELMD provides more useful information about the valve fault than the one obtained by ELMD decomposition. Hence, figures 28 and 29 suggest that the decomposition performance of OELMD is more effective than that of ELMD for the valve fault vibration signal.

4.4. Discussion

The three case studies discussed in this paper demonstrate better performance of OELMD than ELMD due to the determination of suitable critical parameters. Improper ELMD parameters either increase the computation cost, decrease the fault detection performance, or both. Moreover, a suitable number of ensemble trials can be obtained with the
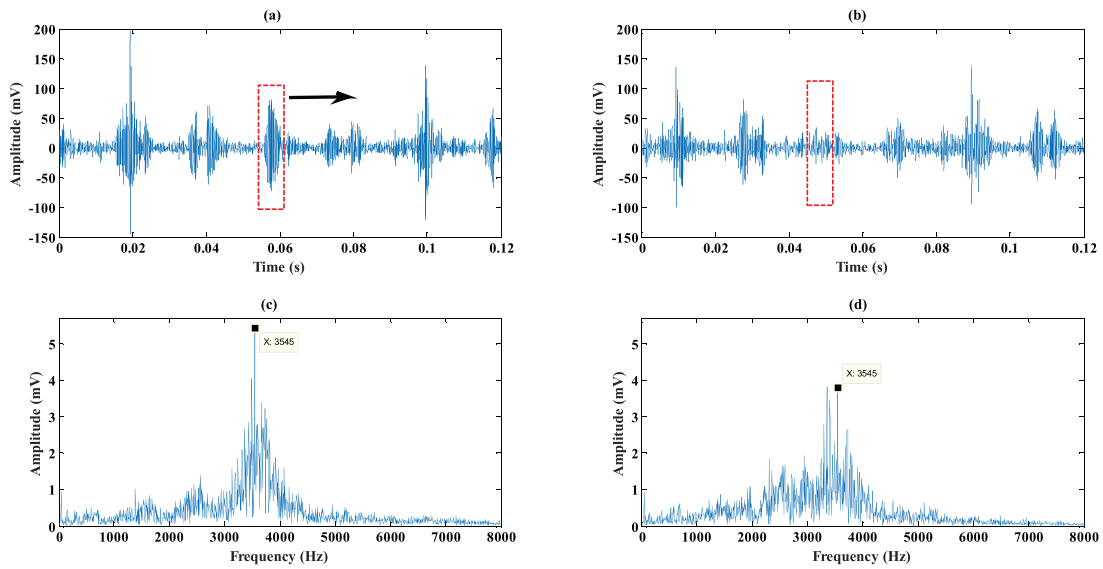
Figure 27. The raw vibration signal: (a) time waveform under the valve fault condition, (b) frequency spectrum under the valve fault condition, (c) time waveform under normal conditions, and (d) frequency spectrum under normal conditions.
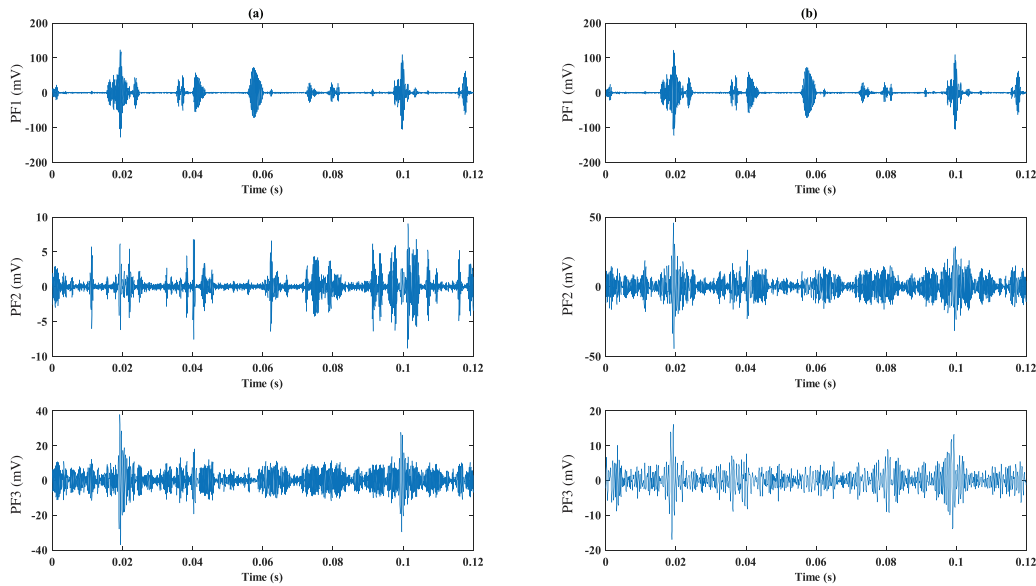

Figure 28. Time waveforms of the first three PFs decomposed by (a) OELMD and (b) ELMD.

OELMD method. The computation cost can be significantly reduced by using the optimized ensemble number while the mode decomposition effectiveness can still be guaranteed. This is because, in most cases, a suitable ensemble number is unknown and large value of the ensemble number is selected for ELMD analysis, artificially and subjectively, for the purpose of reliable mode decomposition. For example, in case study 2, the optimized ensemble number was 50. However, when the original ELMD was used to analyze the signal, it often chose an ensemble number of 100 or more to ensure adequate decomposition performance. Nevertheless, these results do not necessarily mean that OELMD is computationally more efficient than ELMD, because obtaining the optimized parameters also consumes some computational time, which should be considered as part of the computational time required by OELMD. The results only suggest that, after the

suitable ELMD parameters are obtained, the fault detection performance can be improved.

Although an adaptive strategy was proposed to select suitable parameters for EEMD in [16], previous publications indicate better performance of ELMD than EEMD in mechanical fault diagnosis [33–35]. Consequently, in this work, the fault detection performance of OELMD is only compared against ELMD. However, comparisons between OELMD, ELMD, and EEMD have not been conducted on real-world vibration signals. This is an area with practical applications that is worth investigating in future research. In addition, OELMD and ELMD utilize noise to improve the decomposition performance and obtain more distinct fault vibration modes. Another signal processing technique, namely stochastic resonance (SR), also adopts the noise information to enhance fault characteristics [38], and demonstrates promising performance
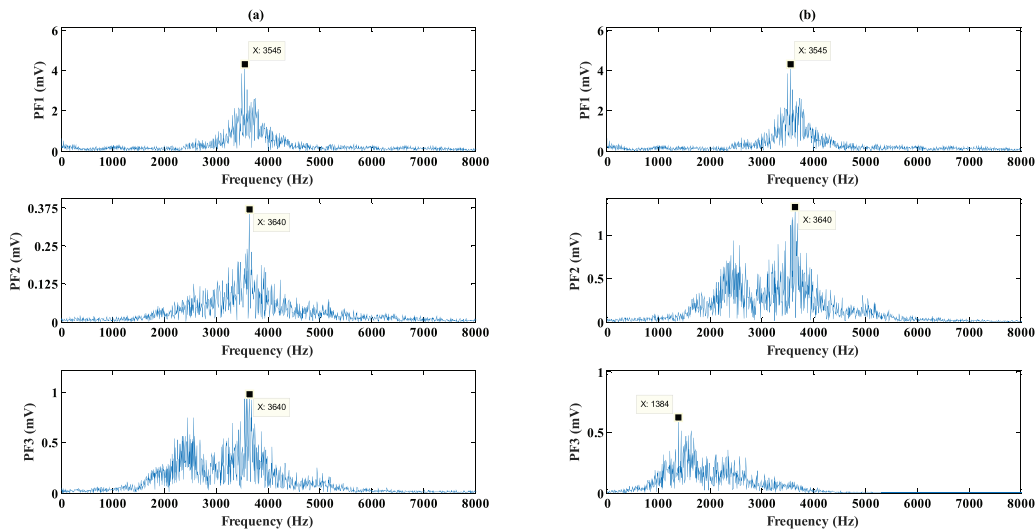
Figure 29. Envelope waveforms of the first three PFs decomposed by (a) OELMD and (b) ELMD.

in fault detection of gearboxes [39]. Hence, our future work will also consider investigating SR-based fault diagnosis on real-world vibration signals and comparing its performance with that of OELMD.

5. Conclusion

In this paper, an ELMD method improved by optimizing three critical parameters, namely OELMD, was proposed. A new procedure based on *Relative RMSE* was introduced to optimize noise amplitude and bandwidth, and a SNR-optimization approach was developed to obtain a suitable ensemble number. When these optimized parameters were applied to the intrinsic mode decomposition process, OELMD can effectively reduce mode mixing and enhance the fault detection performance. Three case studies were conducted to verify the effectiveness of the proposed method. The results demonstrate that (a) suitable ELMD parameters can be obtained by OELMD; (b) OELMD represents an improvement over ELMD in mode mixing reduction, and is therefore expected to increase the fault detection rate; and (c) improvement in computational efficiency is achieved by minimizing the ensemble number. The proposed method has significant practical applications in mechanical fault diagnosis. Our future work will investigate the effectiveness of OELMD with real-world engineering vibration data measured from gearboxes of wind turbines and mining machines, and compare the fault detection performance of OELMD with those of both ELMD and EEMD. SR-based fault diagnosis with the real-world data will also be included in our future research.

Acknowledgments

References

[1] Hreha P, Radvanska A, Knapcikova L, Krolczyk G, Legutko S, Krolczyk J, Hloch S and Monka P 2015 Roughness parameters calculation by means of on-line vibration monitoring emerging from AWJ interaction with material *Metrol. Meas. Syst.* **2** 315–26

[2] Glowacz A and Glowacz Z 2016 Diagnostics of stator faults of the single-phase induction motor using thermal images, MoASoS and selected classifiers *Measurement* **93** 86–93

[3] Wu T, Peng Y, Wu H, Zhang X and Wang J 2014 Full-life dynamic identification of wear state based on on-line wear debris image features *Mech. Syst. Signal Process.* **42** 404–14

[4] Glowacz A 2015 Recognition of acoustic signals of synchronous motors with the use of MoFS and selected classifiers *Meas. Sci. Rev.* **15** 167–75

[5] Li Z and Peng Z 2016 A new nonlinear blind source separation method with chaos indicators for decoupling diagnosis of hybrid failures: a marine propulsion gearbox case with a large speed variation *Chaos Solitons Fractals* **89** 27–39

[6] Hreha P, Radvanska A, Hloch S, Perzel V, Krolczyk G and Monkova K 2015 Determination of vibration frequency depending on abrasive mass flow rate during abrasive water jet cutting *Int. J. Adv. Manuf. Technol.* **77** 763–74

[7] Jiang Y, Zhu H, Li Z and Peng Z 2016 The nonlinear dynamics response of cracked gear system in a coal cutter taking environmental multi-frequency excitation forces into consideration *Nonlinear Dyn.* **84** 203–22

[8] Chaari F, Fakhfakh T and Haddar M 2006 Dynamic analysis of a planetary gear failure caused by tooth pitting and cracking *J. Fail. Anal. Prevention* **6** 73–8

[9] Glowacz A 2015 DC motor fault analysis with the use of acoustic signals, coiflet wavelet transform, and K-nearest neighbor classifier *Arch. Acoust.* **40** 321–7

[10] Li Z, Yan X, Yuan C, Peng Z and Li L 2011 Virtual prototype and experimental research gear multi—fault diagnosis using wavelet—autoregressive model and principal component analysis method *Mech. Syst. Signal Process.* **25** 2589–607

[11] Zhang C, Li B, Cao H, Zi Y, He Z and Chen B 2015 Weak fault signature extraction of rotating machinery using flexible analytic wavelet transform *Mech. Syst. Signal Process.* **64–5** 162–87

[12] Jiang Y, Zhu H and Li Z 2016 A new compound faults detection method for rolling bearings based on empirical wavelet transform and chaotic oscillator *Chaos Solitons Fractals* **89** 8–19

[13] Huang N E *et al* 1998 The empirical mode decomposition and the Hilbert spectrum for nonlinear and non-stationary time series analysis *Proc. R. Soc.* A **454** 903–95

[14] Lei Y, Lin J, He Z and Zuo M J 2013 A review on empirical mode decomposition in fault diagnosis of rotating machinery *Mech. Syst. Signal Process.* **35** 108–26

[15] Wu Z and Huang N E 2009 Ensemble empirical mode decomposition: a noise-assisted data analysis method *Adv. Adapt. Data Anal.* **1** 1–41

[16] Lei Y, Li N, Lin J and Wang S 2013 Fault diagnosis of rotating machinery based on an adaptive ensemble empirical mode decomposition *Sensors* **13** 16950–64

[17] Li Z, Jiang Y, Guo Q, Hu C and Peng Z 2016 Multi-dimensional variational mode decomposition for bearing-crack detection in wind turbines with large driving-speed variations *Renewable Energy* (doi: 10.1016/j.renene.2016.12.013)

[18] Guo W and Tse P 2013 A novel signal compression method based on optimal ensemble empirical mode decomposition for bearing vibration signals *J. Sound Vib.* **332** 423–41

[19] Zhang C, Li Z, Chen S, Wang J and Zhang X 2016 Optimised ensemble empirical mode decomposition with optimised noise parameters and its application to rolling element bearing fault diagnosis *Insight* **58** 494–501

[20] Sanchez J, Ortigueira M, Rato R and Trujillo J 2016 An improved empirical mode decomposition for long signals *Proc. of the 1st Int. Conf. on Advances in Signal, Image and Video Processing* (*Lisbon, Portugal*, *26–30 June 2016*) pp 58–62

[21] Stepien P 2014 Sliding window empirical mode decomposition–its performance and quality *EPJ Nonlinear Biomed. Phys.* **2** 2–14

[22] Smith J 2005 The local mean decomposition and its application to EEG perception data *J. R. Soc. Interface* **2** 443–54

[23] Cheolsoo P, David L, Marc M and Danilo P 2011 The complex local mean decomposition *Neurocomputing* **74** 867–75

[24] Wang Y, He Z and Zi Y 2009 A demodulation method based on improved local mean decomposition and its application in rub-impact fault diagnosis *Meas. Sci. Tech.* **20** 025704

[25] Wang Y, He Z and Zi Y 2010 A comparative study on the local mean decomposition and empirical mode decomposition and their applications to rotating machinery health diagnosis *J Vib. Acoust.* **132** 021010

[26] Wang Y, He Z, Xiang J and Zi Y 2012 Application of local mean decomposition to the surveillance and diagnostics of low-speed helical gearbox *Mech. Mach. Theory* **47** 62–73

[27] Kidar T, Thomas M, Guilbault R and El B 2013 Comparison between the efficiency of LMD and EMD algorithms for early detection of gear defects *Mech. Ind.* **14** 121–7

[28] Feng Z, Zuo M, Qu J, Tian T and Liu Z 2013 Joint amplitude and frequency demodulation analysis based on local mean decomposition for fault diagnosis of planetary gearboxes *Mech. Syst. Signal Process.* **40** 56–75

[29] Cheng J, Yang Y and Yang Y 2012 A rotating machinery fault diagnosis method based on local mean decomposition *Dig. Signal Process.* **22** 356–66

[30] Liu Z, He Z, Guo W and Tang Z 2016 A hybrid fault diagnosis method based on second generation wavelet de-noising and local mean decomposition for rotating machinery *ISA Trans.* **61** 211–20

[31] Han M and Pan J 2015 A fault diagnosis method combined with LMD, sample entropy and energy ratio for roller bearings *Measurement* **76** 1–19

[32] Jang W, Zheng Z, Zhu Y and Li Y 2015 Demodulation for hydraulic pump fault signals based on local mean decomposition and improved adaptive multiscale morphology analysis *Mech. Syst. Signal Process.* **58–9** 179–205

[33] Sun J, Xiao Q, Wen J and Zhang Y 2015 Natural gas leak location with K–L divergence-based adaptive selection of ensemble local mean decomposition components and high-order ambiguity function *J. Sound Vib.* **347** 232–245

[34] Yang Y, Cheng J and Zhang K 2012 An ensemble local mean decomposition method and its application to local rub-impact fault diagnosis of the rotor systems *Measurement* **45** 561–70

[35] Cheng J, Zhang K and Yang Y 2011 Ensemble local mean decomposition method based on noise-assisted analysis *J. Mech. Eng.* **47** 55–62

[36] Xue X, Zhou J, Xu Y, Zhu W and Li C 2015 An adaptively fast ensemble empirical mode decomposition method and its applications to rolling element bearing fault diagnosis *Mech. Syst. Signal Process.* **62–3** 444–59

[37] Randall R and Antoni J 2011 Rolling element bearing diagnostics—a tutorial *Mech. Syst. Signal Process.* **25** 485–520

[38] Nishiguchi K and Fujiwara A 2012 Detecting signals buried in noise via nanowire transistors using stochastic resonance *Appl. Phys. Lett.* **101** 193108

[39] Qiao Z, Lei Y, Lin J and Jia F 2017 An adaptive unsaturated bistable stochastic resonance method and its application in mechanical fault diagnosis *Mech. Syst. Signal Process.* **84** 731–46